Single-Period Floquet Control of Bosonic Codes with Quantum Lattice Gates

Downloaded from: https://research.chalmers.se, 2026-11-16 12:46 UTC

Citation for the original published paper (version of record):
Huang, T., Du, L., Guo, L. (2026). Single-Period Floquet Control of Bosonic Codes with Quantum Lattice Gates. Physical Review Letters, 137(6). http://dx.doi.org/10.1103/tnb8-3m8m

N.B. When citing this work, cite the original published paper.

research.chalmers.se offers the possibility of retrieving research publications produced at Chalmers University of Technology. It covers all kind of research output: articles, dissertations, conference papers, reports etc. since 2004. research.chalmers.se is administrated and maintained by Chalmers Library

(article starts on next page)

Single-Period Floquet Control of Bosonic Codes with Quantum Lattice Gates

Tangyou Huang,[1] Lei Du,[1,*] and Lingzhen Guo[2,3,†]

[1]Department of Microtechnology and Nanoscience (MC2), Chalmers University of Technology, SE-41296 Göteborg, Sweden
[2]Center for Joint Quantum Studies and Department of Physics, School of Science, Tianjin University, Tianjin 300072, China
[3]Tianjin Key Laboratory of Low Dimensional Materials Physics and Preparing Technology, Department of Physics, Tianjin University, Tianjin 300354, China

(Received 8 January 2026; revised 20 April 2026; accepted 22 June 2026; published 3 August 2026)

Bosonic codes constitute a promising route to fault-tolerant quantum computing. Existing Floquet protocols enable analytical construction of bosonic codes but typically rely on slow adiabatic ramps with thousands of driving periods. In this Letter, we circumvent this bottleneck by introducing an analytical and deterministic Floquet method that directly synthesizes arbitrary unitaries within a single period. The phase-space unitary ensembles generated by our approach reproduce the Haar-random statistics, enabling practical pseudorandom states in continuous-variable systems. We prepare various prototypical bosonic codes from vacuum and implement single-qubit logical gates with high fidelities using quantum lattice gates. By harnessing the full intrinsic nonlinearity of Josephson junctions, quantum lattice gates decompose quantum circuits into primitive operations for efficient continuous-variable quantum computing.

DOI: 10.1103/tnb8-3m8m

Introduction—Fault-tolerant quantum computation promises advantages over its classical counterpart, ranging from fundamental research to commercial applications. Practical fault tolerance typically relies on quantum error correction (QEC) [1], which has been experimentally demonstrated across discrete-variables (DV) and continuous-variables (CV) platforms [2,3], as well as in hybrid DV-CV architectures [4]. Unlike the DV cases, CV protocols leverage the infinite-dimensional Hilbert space of harmonic oscillators, offering redundancy in encoding quantum information without the need for large numbers of physical qubits [5,6].

A universal set of single-mode CV quantum gates can be realized using Gaussian operations, such as displacements, squeezing, and phase rotations, in combination with a single nonlinear operation such as the cubic phase gate [7]. In superconducting circuits, the cubic phase gate has been demonstrated using an on-chip planar resonator terminated by a SNAIL element [8,9]. Another popular single-mode universal gate set combines displacements with the selective number-dependent arbitrary phase (SNAP) gates, which impart arbitrary phases to individual Fock states via an off-resonantly coupled ancilla transmon qubit [10–12]. The universal gate set for multimode CV quantum computation requires only the inclusion of a simple two-mode linear coupling [13,14]. However, universality alone is not sufficient for fault-tolerant quantum computation. On the one hand, the continuous nature of bosonic-quadrature errors necessitates embedding a finite-dimensional code space within the infinite-dimensional CV Hilbert space [15]. On the other hand, non-Gaussian resources are typically required to correct Gaussian errors [16] and implement fault-tolerant quantum computation [17,18]. When the encoded states satisfy the Knill-Laflamme conditions [19], they realize bosonic QEC codes [20–22].

Both the cubic phase gate and the SNAP gate need complicated design of superconducting circuits using the low-order nonlinearity of Josephson junctions (JJs) [23]. In contrast, the recently introduced *quantum lattice gates* (QLGs) leverage the full nonlinearity of JJ superconducting circuits and can provide an analytical framework based on the Floquet engineering to prepare and manipulate bosonic codes [24]. However, this approach suffers from slow adiabatic ramps [24,25] costing thousands of Floquet periods, which severely limits the speed and practical scalability for universal quantum computation.

In this Letter, we overcome this bottleneck by introducing an analytical, deterministic Floquet-engineering method that directly synthesizes arbitrary bosonic unitaries from an arbitrary initial state within a *single* Floquet period. We validate our method by generating gate ensembles whose fidelity statistics reproduce those of Haar-random states [26]. The numerical results show that, for Haar-state preparation, the computational resources required by our method scale linearly with the Hilbert-space dimension, with a substantially smaller prefactor than the SNAP-based

*Contact author: lei.du@chalmers.se
†Contact author: lingzhen_guo@tju.edu.cn

Published by the American Physical Society under the terms of the Creative Commons Attribution 4.0 International license. Further distribution of this work must maintain attribution to the author(s) and the published article's title, journal citation, and DOI. Funded by Bibsam.

approach. We further develop an *optimal pulse engineering* (OPE) technique to prepare binomial [27], cat [4,28], and Gottesman-Kitaev-Preskill (GKP) [29] codes directly from vacuum, achieving state infidelities below 10^{-5}. Furthermore, we demonstrate high-fidelity logical gates for these representative bosonic codes, with average gate errors on the order of 10^{-4}, in *few-microsecond* QLGs, which is over three orders of magnitude faster than existing adiabatic protocols [24,25,30].

Noncommutative Floquet engineering—From the Floquet theory, the stroboscopic evolution over one period of a time-periodic Hamiltonian $\hat{H}(t) = \hat{H}(t+T)$ is captured by a time-independent Floquet Hamiltonian $\hat{H}_{\mathrm{F}}$ [31–33],

$$\exp\left(-i\frac{1}{\lambda}\hat{H}_{\mathrm{F}}T\right) \equiv \mathcal{T}\exp\left[-\frac{i}{\lambda}\int_0^T \hat{H}(t)dt\right], \quad (1)$$

where λ is an effective dimensionless Planck constant, T is the Floquet period, and $\mathcal{T}$ is the time-ordering operator. In this Letter, we consider a driven cavity described by $\hat{H}_{\mathrm{cav}}/(\hbar\omega_0) = \hat{a}^\dagger\hat{a} + \hat{V}(t)$ [30], where $\hat{a}$ ($\hat{a}^\dagger$) is the annihilation (creation) operator of the cavity. Our objective is to realize an arbitrary unitary operation on a d-dimensional subspace of cavity mode. For any target unitary operator $\hat{U}_{\mathrm{tar}} \in \mathbb{U}(d)$, there exists a Hermitian generator $\hat{H}_{\mathrm{tar}}$ such that $\hat{U}_{\mathrm{tar}} = e^{-i\hat{H}_{\mathrm{tar}}/\lambda}$. The key idea is to design a periodic potential $\hat{V}(t)$ for synthesizing an arbitrary Floquet Hamiltonian in the cavity-frequency rotating frame $\hat{H}_{\mathrm{tar}} = \sum_{j,l}\epsilon_{j,l}(\hat{a}^\dagger)^j\hat{a}^l$, where $\epsilon_{j,l} = \epsilon^*_{l,j} \in \mathbb{C}$ denote the complex driving amplitudes. We write the target Hamiltonian in the orthonormal Fock basis $\{|n\rangle\}_{n=0}^{d-1}$ as $\hat{H}_{\mathrm{tar}} = \sum_{n,m=0}^{d-1} h_{n,m}|n\rangle\langle m|$ with $h_{n,m} = \langle n|\hat{H}_{\mathrm{tar}}|m\rangle$.

According to the technique of *noncommutative Fourier transformation* (NcFT) [30], the target Hamiltonian is decomposed as a superposition of plane-wave operators,

$$\hat{H}_{\mathrm{tar}}(\hat{x},\hat{p}) = \frac{1}{2\pi}\int\int dk_x dk_p f_{\mathrm{tar}}(k_x,k_p)e^{i(k_x\hat{x}+k_p\hat{p})}. \quad (2)$$

Here, the quadrature operators are defined as $\hat{x} \equiv \sqrt{(\lambda/2)}(\hat{a}^\dagger + \hat{a})$ and $\hat{p} \equiv i\sqrt{(\lambda/2)}(\hat{a}^\dagger - \hat{a})$, which satisfy $[\hat{x},\hat{p}] = i\lambda$. k_x and k_p are phase-space Fourier variables associated with quadratures $\hat{x}$ and $\hat{p}$, and $e^{i(k_x\hat{x}+k_p\hat{p})}$ can be viewed as a phase-space displacement generator. By introducing the variables $k \equiv \sqrt{k_x^2+k_p^2}$ and $\tau \equiv \omega_0 t = \mathrm{Arg}(k_x + ik_p)$, the NcFT coefficient f_{tar} is given in the Fock basis by

$$f_{\mathrm{tar}}(k,\tau) = \sum_{n,m} h_{n,m} f_{n,m}(k,\tau). \quad (3)$$

The explicit kernels $f_{n,m}(k,\tau)$ are given in Supplemental Material [34]. With the NcFT coefficient, the synthesized driving potential can be written as a superposition of cosine-type potentials [30]

$$\hat{V}(\hat{x},\tau) = \int_{-\infty}^{+\infty} \beta_0 A(k,\tau)\cos[k\hat{x} + \phi(k,\tau)]dk, \quad (4)$$

where the target-independent parameter β_0 controls the driving strength. The time-dependent amplitude $A(k,\tau)$ and phase $\phi(k,\tau)$ are given by

$$\begin{cases} A(k,\tau) = k|f_{\mathrm{tar}}(k\cos\tau, k\sin\tau)|, \\ \phi(k,\tau) = \mathrm{Arg}[f_{\mathrm{tar}}(k\cos\tau, k\sin\tau)]. \end{cases} \quad (5)$$

As shown in Eq. (4), the target potential is synthesized by superposing the cosine-type components with $A(k,\tau)$ and $\phi(k,\tau)$. Experimentally, each cosine component can be physically implemented, for example, with optical lattices in ultracold atom setups [47], or JJ potentials in superconducting circuits [48]. To the leading order in the Floquet-Magnus (FM) expansion, the target unitary operator is given by the rotating-frame driving potential as follows

$$\hat{U}_{\mathrm{tar}} \approx \mathcal{T}\exp\left[-\frac{i}{\lambda}\int_0^T \hat{V}(\tau)d\tau\right]. \quad (6)$$

In principle, higher-order FM errors can be mitigated by adding driving terms perturbatively [49].

Quantum lattice gate—In our protocol, we approximate the target unitary [Eq. (6)] by a Trotter-Suzuki (TS) decomposition of the driving potential [Eq. (4)], which leads to a sequence of QLGs [24],

$$\hat{\mathbf{G}}(\vec{\theta},\vec{\gamma}) \equiv \prod_{m=1}^{N_t}\left[e^{-i\frac{T}{N_t}\hat{a}^\dagger\hat{a}}\prod_{n=1}^{N_k}\hat{\mathbf{g}}(\theta_{n,m},\gamma_{n,m})\right] \quad (7)$$

with N_t (N_k) the number of discretization steps, i.e., the Trotter depth, for time (wave number), and $\hat{\mathbf{g}}(\theta_{n,m},\gamma_{n,m})$ the elementary QLG defined via

$$\hat{\mathbf{g}}(\theta_{n,m},\gamma_{n,m}) \equiv e^{-\frac{i}{\lambda}\theta_{n,m}\cos(k_n\hat{x}+\gamma_{nm})}. \quad (8)$$

Here, we have introduced parameters $\gamma_{n,m} = \phi(k_n,\tau_m)$, $\theta_{n,m} = \beta_0 A(k_n,\tau_m)(T/N_t)(k_f/N_k)$ with $\tau_m = m(T/N_t)$, $k_n = n(k_f/N_k)$, where k_f is an appropriate cutoff for the wave number. Except for errors from the high-order FM expansion, another error of $\hat{\mathbf{G}}(\vec{\theta},\vec{\gamma})$ approximating the target unitary $\hat{U}_{\mathrm{tar}}$ originates from the TS decomposition [cf. Eq. (7)], which can be suppressed by employing higher-order TS expansions and adaptive optimization strategies [50–52]. In this way, an arbitrary target unitary U_{tar} acting on a truncated d-dimensional Fock space can be synthesized, within a single Floquet period, by a sequence of QLGs.

Single-period Floquet control with QLGs—We first apply our protocol to prepare a target state $|\psi_{\mathrm{tar}}\rangle$ from a known initial state $|\psi_0\rangle$ via a unitary, i.e., $|\psi_{\mathrm{tar}}\rangle = \hat{U}_{\mathrm{tar}}|\psi_0\rangle$. We exclude the trivial case $|\psi_{\mathrm{tar}}\rangle = e^{i\eta}|\psi_0\rangle$ for some global phase η. Previous approaches based on adiabatic ramping suffer from intrinsic limitations: maintaining adiabaticity requires a sufficiently slow Hamiltonian variation, which typically results in evolution over thousands of Floquet periods [24,25,30]. In this Letter, we use a Householder-based construction [35,53] to obtain a closed-form unitary that maps the known initial state $|\psi_0\rangle$ to the target state $|\psi_{\mathrm{tar}}\rangle$, without the need for any adiabatic processes. In Supplemental Material [34], we provide details on the Householder-based construction and discuss alternative unitary construction methods. By defining the normalized Householder vector $|u\rangle \equiv (|\psi_0\rangle - e^{i\varphi}|\psi_{\mathrm{tar}}\rangle)/\||\psi_0\rangle - e^{i\varphi}|\psi_{\mathrm{tar}}\rangle\|$ with $e^{i\varphi} \equiv \langle\psi_{\mathrm{tar}}|\psi_0\rangle/|\langle\psi_{\mathrm{tar}}|\psi_0\rangle|$ (setting $e^{i\varphi} = 1$ if $\langle\psi_{\mathrm{tar}}|\psi_0\rangle = 0$), the target unitary can be obtained explicitly as

$$\hat{U}_{\mathrm{tar}} = \left[\hat{I} + (e^{-i\varphi} - 1)|\psi_{\mathrm{tar}}\rangle\langle\psi_{\mathrm{tar}}|\right]\left(\hat{I} - 2|u\rangle\langle u|\right), \quad (9)$$

where $\hat{I}$ is the identity operator. It is straightforward to verify that $\hat{U}_{\mathrm{tar}}|\psi_0\rangle = |\psi_{\mathrm{tar}}\rangle$, while $\hat{U}_{\mathrm{tar}}$ acts as the identity (up to an overall phase) on the subspace orthogonal to the space spanned by $|\psi_0\rangle$ and $|\psi_{\mathrm{tar}}\rangle$. Such $\hat{U}_{\mathrm{tar}} = e^{-i\hat{H}_{\mathrm{tar}}/\lambda}$ can then be decomposed into a sequence of elementary QLGs using the Floquet Hamiltonian engineering described above.

In Fig. 1, we illustrate the workflow for preparing arbitrary target states $|\psi_{\mathrm{tar}}\rangle$ from the vacuum $|\psi_0\rangle = |0\rangle$ using QLGs. Starting from a randomly chosen nonclassical state, with its Wigner function shown in Fig. 1(a), we first construct the target unitary $\hat{U}_{\mathrm{tar}}$ using the unitary-construction scheme, cf. Eq. (9), with arbitrary high fidelity $\mathcal{F} = |\langle\psi_{\mathrm{tar}}|\hat{U}_{\mathrm{tar}}|\psi_0\rangle|^2$ (limited only by the machine precision in our simulation) [34]. The corresponding target Hamiltonian obtained via $\hat{H}_{\mathrm{tar}} = i\lambda\log(\hat{U}_{\mathrm{tar}}) \equiv \sum_{n,m} h_{n,m}|n\rangle\langle m|$ is visualized in Fig. 1(b). Next, from the NcFT representation of $\hat{H}_{\mathrm{tar}}$, cf. Eqs. (2)–(4), we deterministically obtain the time-dependent driving amplitude and phase $A(k,\tau)$ and $\phi(k,\tau)$, as shown in Fig. 1(c). Finally, the driving potential is decomposed into a sequence of QLG operations given by Eq. (7). Figure 1(d) shows how the state-preparation fidelity depends on the discretization parameters $\{N_t, N_k\}$. For the example shown, our approach prepares the target states with fidelity $\gtrsim 0.99$ using $N_t = 2^6$, $N_k = 40$ and $d = 15$. Moreover, Fig. 1(d) shows that the Trotter error associated with N_k is less pronounced than the error from the time slicing N_t. We therefore vary N_t while holding N_k fixed for subsequent benchmarks. Note that the entire preparation is completed within a single Floquet period, indicating that our approach is at least three orders of magnitude faster than the adiabatic ramp method

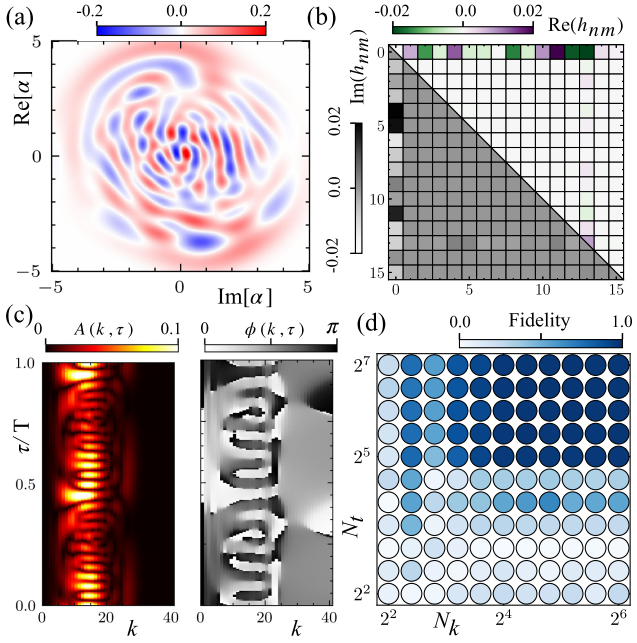

FIG. 1. Single-period Floquet control with QLGs. (a) Wigner function of the target state $|\psi_{\mathrm{tar}}\rangle$. (b) Target Hamiltonian $\hat{H}_{\mathrm{tar}} = i\lambda\log(\hat{U}_{\mathrm{tar}})$ in the Fock basis, where the target unitary $\hat{U}_{\mathrm{tar}}$ is constructed from Eq. (9). (c) Amplitude $A(k,\tau)$ and phase $\phi(k,\tau)$ of the driving potential over one Floquet period T. (d) State-preparation fidelity $\mathcal{F} = |\langle\psi_{\mathrm{tar}}|\hat{U}_{\mathrm{tar}}|\psi_0\rangle|^2$ as a function of Trotter depths N_k and N_t. We use $N_t = 2^6$ and $N_k = 40$ in (a)–(c). Other parameters: $N_p = 15$, $k_f = 40$, and $\beta_0 = 1$.

[24,25,30]. A detailed comparison of our method with previous protocols is provided in the End Matter.

Haar-random state benchmark—Haar-typical states and unitaries serve as a widely used benchmark for assessing quantum controllability in high-dimensional Hilbert spaces. In this context, we sample targets from the Haar measure and examine whether the implemented operations faithfully reproduce the statistics of Haar randomness [54]. Such pseudorandom behavior underlies a broad range of quantum information protocols and can be realized using gate-based quantum circuits [55] and CV schemes involving non-Gaussian resources [56,57].

Here, we construct a QLG-based unitary generator on a d-dimensional subspace whose output matches Haar statistics in phase space. Concretely, we define Haar-random states $|\psi_{\mathrm{Haar}}\rangle \equiv \hat{U}_{\mathrm{Haar}}|0\rangle$ drawn from the Haar measure on the unit sphere in $\mathbb{C}^d$ [34], and study the distribution of fidelities with respect to a reference Haar state $|\psi_{\mathrm{ref}}\rangle$. For an ensemble of Haar-distributed pure states, the fidelity $\mathcal{F} = |\langle\psi_{\mathrm{Haar}}|\psi_{\mathrm{ref}}\rangle|^2$ is a variable following the probability density function [54]

$$\mathbb{P}_{\mathrm{Haar}}(\mathcal{F}) = (d-1)(1-\mathcal{F})^{d-2}, \quad (10)$$

with the mean fidelity $\mathbb{E}[\mathcal{F}] = 1/d$. In our implementation, we take each sampled $|\psi_{\mathrm{Haar}}\rangle$ as the target state and

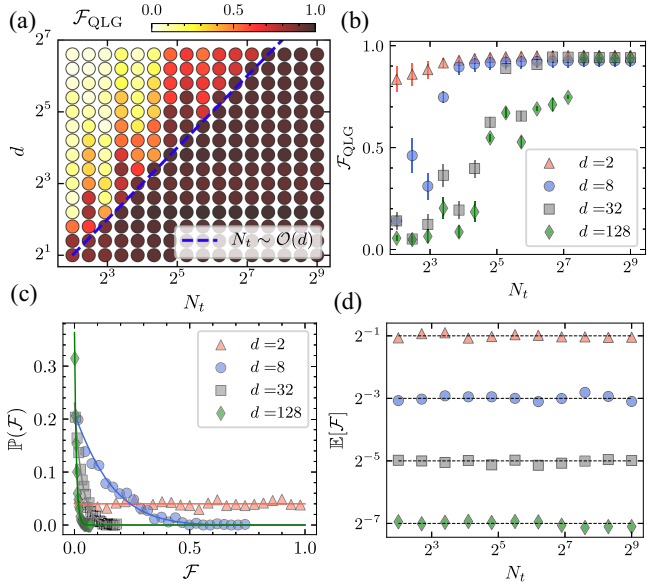

FIG. 2. Haar-random state benchmark. (a) Average fidelity $\mathcal{F}_{\rm QLG} \equiv |\langle\psi_{\rm QLG}|\psi_{\rm Haar}\rangle|^2$ of Haar-state preparation versus Trotter depth N_t and Hilbert subspace dimension d, where each marker is averaged over 10^2 randomly sampled Haar unitaries. The blue dashed line indicates the empirical scaling $N_t \sim \mathcal{O}(d)$ required to reach high fidelity ($\mathcal{F}_{\rm QLG} \gtrsim 0.95$). (b) Fidelity $\mathcal{F}_{\rm QLG}$ versus N_t for different dimensions d (10^3 samples per point). (c) Probability density distribution $\mathbb{P}(\mathcal{F})$ of the stochastic fidelity $\mathcal{F} = |\langle\psi_{\rm QLG}|\psi_{\rm ref}\rangle|^2$ over $10^2 \times d$ QLG realizations (markers) compared with the analytical Haar statistics $\mathbb{P}_{\rm Haar}(\mathcal{F})$ given by Eq. (10) (solid curves) for different dimensions. (d) Mean fidelity $\mathbb{E}[\mathcal{F}]$ versus N_t, with the theoretical prediction $1/d$ shown as dashed lines. Other parameters are the same as in Fig. 1.

construct the target unitary $\hat{U}_{\rm Haar}$ from Eq. (9) with the initial vacuum state $|0\rangle$. We then design a sequence of QLGs from Eq. (7) for each target unitary $\hat{U}_{\rm Haar}$ yielding

$$|\psi_{\rm QLG}\rangle = \hat{\mathbf{G}}_{\rm Haar}(\vec{\theta},\vec{\gamma})|0\rangle, \tag{11}$$

which approximates the sampled Haar state $|\psi_{\rm Haar}\rangle$ with high fidelity $\mathcal{F}_{\rm QLG} \equiv |\langle\psi_{\rm QLG}|\psi_{\rm Haar}\rangle|^2$.

Figure 2(a) shows the average fidelity $\mathcal{F}_{\rm QLG}$ of Haar-state preparation using QLGs as a function of the Hilbert subspace dimension d and the Trotter depth N_t. The blue dashed line indicates the empirical scaling $N_t \sim \mathcal{O}(d)$ required to reach high fidelity ($\mathcal{F}_{\rm QLG} \gtrsim 0.95$). As further illustrated by Fig. 2(b), choosing $N_t = 2d$ yields $\mathcal{F}_{\rm QLG} \gtrsim 0.98$ for $d = 2$, 8, 32, 128. This overhead can be further reduced by higher-order TS formulas [58] and numerical optimization [51], which we leave for future work. In Fig. 2(c), we calculate the fidelity $\mathcal{F} = |\langle\psi_{\rm QLG}|\psi_{\rm ref}\rangle|^2$ with respect to a fixed reference Haar state and plot the probability density distributions $\mathbb{P}(\mathcal{F})$ for different subspace dimensions, which are consistent with the Haar statistics given by Eq. (10). Figure 2(d) further shows the mean fidelity as a function of N_t. All curves approach the theoretical value $1/d$ with only weak dependence on the Trotter depth, indicating that the QLG protocol preserves the Haar statistics. These results show that our QLG approach reproduces Haar-like statistics faithfully, and thus can serve as a practical generator of pseudorandom states. We also benchmark our method against a SNAP-gate-based construction in the End Matter.

Bosonic codes preparation and logical operations—We next validate our QLG approach by demonstrating the preparation of binomial [36], cat [4], and GKP codes [29], see a brief introduction to these prototypical bosonic codewords in the SM [34]. Here, we focus on the preparation of the logical zero code states, i.e., the binomial code $|\psi_{\rm bin}\rangle = (|0\rangle + \sqrt{3}|4\rangle)/2$ and the four-component cat code $|\psi_{\rm cat}\rangle = (1/\sqrt{\mathcal{N}_{\rm cat}})(|\alpha\rangle + |-\alpha\rangle + |i\alpha\rangle + |-i\alpha\rangle)$ with (real) coherent-state amplitude α and normalization factor $\mathcal{N}_{\rm cat} = 8e^{-\alpha^2}[\cosh\alpha^2 + \cos\alpha^2]$. Hereafter we choose the second sweet spot $\alpha = 2.3447$ for the cat state, which satisfies Knill-Laflamme condition $\tan\alpha^2 = \tanh\alpha^2$ [19,34,37]. For the finite-energy GKP code parametrized by a real width parameter $\sigma \in [0,1]$, we use its Fock-basis form $|\psi_{\rm GKP}\rangle = \sum_{\alpha'\in\mathcal{K}(\mu)} e^{-\sigma^2|\alpha'|^2} e^{-i{\rm Re}[\alpha']\,{\rm Im}[\alpha']}\hat{\mathcal{D}}(\alpha')|0\rangle$, where $\hat{\mathcal{D}}(\alpha')$ is the displacement operator. The complex amplitude α' is chosen from the discrete grid $\mathcal{K}(\mu) = (\sqrt{\pi/2})(2n_1+\mu) + i(\sqrt{\pi/2})n_2$, with $\mu \in \{0,1\}$ the logical index, and (n_1,n_2) spanning a finite integer range. The Gaussian envelope $e^{-\sigma^2|\alpha'|^2}$ imposes a finite-energy constraint, while the phase factor $e^{-i{\rm Re}[\alpha']\,{\rm Im}[\alpha']}$ ensures the correct symplectic structure in phase space [34].

Moreover, our approach enables single-qubit logical gate operations on the subspace spanned by the two bosonic code states. In particular, arbitrary target single-qubit unitaries $\hat{\mathcal{G}}_{\rm tar} \in \mathbb{SU}(2)$ on the two-dimensional logical space can be synthesized via QLGs for the different bosonic codes introduced above. According to the *Solovay-Kitaev theorem* [59], any single-qubit unitary can be approximated to ε error using $O[\log^c(1/\varepsilon)]$ gates with a constant $c \approx 2$. For instance, the set of Hadamard (H), phase (S) and $\pi/8$ (T) gates constitutes a standard basis for universal quantum computation; within our framework these gates compile to QLGs for all three codes mentioned above. To quantify the performance of the QLGs-compiled single-qubit gate $\hat{\mathcal{G}}_{\rm QLG}$, we benchmark on the logical subspace using the average gate fidelity defined by [60,61]

$$\mathcal{F}_{\rm gate} \equiv \frac{|{\rm Tr}(\hat{\mathcal{G}}_{\rm tar}^\dagger \hat{\mathcal{G}}_{\rm QLG})|^2 + d'}{d'(d'+1)}, \tag{12}$$

where d' is the logical-subspace dimension (e.g., $d' = 2$ for a qubit) and the effective logical gate realized by the sequence of QLGs evolution is $\hat{\mathcal{G}}_{\rm QLG} = \hat{Q}^\dagger \hat{\mathbf{G}}(\vec{\theta},\vec{\gamma})\hat{Q}$, where

$\hat{Q}$ maps the physical Hilbert space to the logical basis (for details see Ref. [34]).

OPE—We finally develop a numerical pulse engineering optimization method to optimally mitigate both the high-order FM errors and the TS errors under specific hardware constraints. To this end, we replace the constant driving strength β_0 in Eq. (4) by a time-dependent envelope $\beta(\tau) \in \mathbb{R}$ used for optimal control. Over one period T, we discretize $\beta(\tau)$ into N_t slices, i.e., $\vec{\beta} = \{\beta_1, \ldots, \beta_{N_t}\}$, and then solve

$$\min_{\vec{\beta} \in \mathbb{R}^{N_t}} \mathcal{L}(|\psi_{\mathrm{QLG}}(\vec{\beta})\rangle, |\psi_{\mathrm{tar}}\rangle)$$
$$\text{subject to } |\vec{\beta} - \vec{\beta}_0| \leq \delta, \tag{13}$$

where $\mathcal{L}(\cdot)$ is the task-specific loss [for state preparation, $\mathcal{L} = 1 - |\langle\psi_{\mathrm{tar}}|\psi_{\mathrm{QLG}}(\vec{\beta})\rangle|^2$; for logical gates, $\mathcal{L} = 1 - \mathcal{F}_{\mathrm{gate}}$. The bound $\delta > 0$ encodes the maximum admissible amplitude feasibility set by the hardware. The discrete envelope $\vec{\beta}$ is initialized as $\vec{\beta}_0 = \{\beta_0, \beta_0, \ldots, \beta_0\} \in \mathbb{R}^{\times N_t}$ with $\beta_0 = 1/\omega_0$ and then optimized with a gradient-based method; see more details in [34].

Figures 3(a) and 3(b) illustrate the preparation of binomial, cat, and GKP codewords from the vacuum using OPE-based QLGs for different Trotter depths and control bounds. Figure 3(a) shows that the infidelity $1 - \mathcal{F}$ decreases rapidly as N_t increases up to 2^6 and eventually saturates around 10^{-6}. Figure 3(b) shows code-dependent convergence behaviors of the optimal control improved by relaxing the control bound. Specifically, optimal control reduces the infidelity from $\sim 10^{-2}$ to below $\sim 10^{-5}$ for $\delta/\beta_0 \geq 0.5$. These results show that high-fidelity bosonic-code preparation is feasible, with the performance governed by both the Trotter depth and the control bounds. In Fig. 3(c), we randomly sample 10^2 target single-qubit logical gates $\hat{\mathcal{G}}_{\mathrm{tar}} \in \mathbb{SU}(2)$, and show the distribution of the gate infidelity with a violin plot (colored region) for each bosonic code. The three violin plots are unimodal with narrow interquartile ranges (below 10^{-1}) and medians ranging from $\sim 10^{-2}$ to $\sim 10^{-3}$, indicating that our QLG protocol is statistically stable across targets. Moreover, as shown in Fig. 3(d), all the three codes realize the elementary gates {H, S, T} with gate errors $\lesssim 10^{-4}$ with optimal control, which are comparable to the state-of-the-art performance of superconducting single-qubit gates [62,63].

Discussion and conclusion—In summary, we present an analytical single-period Floquet protocol of bosonic codes with quantum lattice gates, avoiding slow adiabatic ramps over thousands of periods [24,25] and the global variational searches as in SNAP-based approaches [11,64]. Within this framework, we numerically demonstrate high-fidelity preparation of Haar-distributed target states and employ Haar-statistics benchmarks to assess the controllability of our single-period Floquet control via QLGs. By combining QLGs with optimal pulse engineering, we achieve high-fidelity preparation of binomial, cat, and GKP codewords and universal logical single-qubit gates.

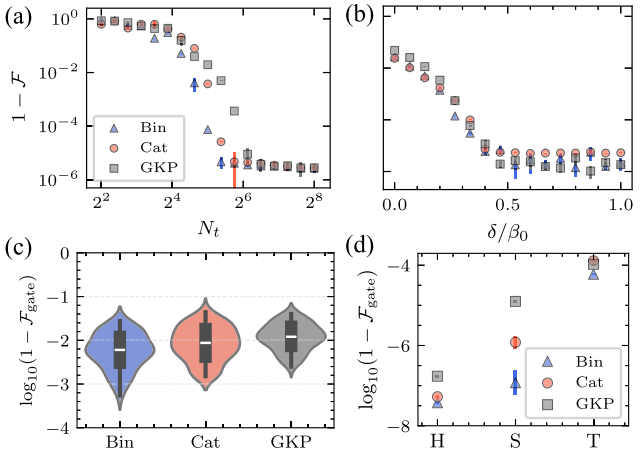

FIG. 3. Bosonic code preparation and operation. (a),(b): Infidelity of prepared code states versus (a) Trotter depth N_t and (b) control bound δ/β_0 for the binomial (triangle), cat (circle), and GKP (square) codes. (c) Violin plots for the binomial (Bin), Cat, and GKP codes by randomly sampling over 10^2 logical gates. The width of each violin (colored region) for a given infidelity logarithm value $\log_{10}(1 - \mathcal{F}_{\mathrm{gate}})$ is proportional to the probability density of the infidelity. The white line marks the median and the black box represents the interquartile range. (d) Infidelity of elementary single-qubit gates {H, S, T} realized via quantum optimal control for each code. The error bars indicate standard deviation over 10^2 data points. Parameters: $\delta = 1$ for (a), $N_t = 2^6$ for (b), and $N_t = 2^8$, $\delta = 2$ for (c),(d). Other parameters follow Fig. 1.

In the End Matter, we further compare our method with an adiabatic-ramping-based protocol in terms of timescale, fidelity, and noise robustness. Our single-period method significantly outperforms this adiabatic protocol, yielding improvements of up to three orders of magnitude across all considered metrics. We also present a numerical controllability benchmark comparing the QLG and SNAP protocols. This benchmark shows that the computational resources required by our method scale linearly with the Hilbert-space dimension, and that the QLG *Ansatz* achieves the target accuracy with fewer resources and substantially faster optimization convergence than the SNAP *Ansatz*.

The impact of coherent noise and decoherence is analyzed in Supplemental Material [34], where the short, single-period operation times are shown to enable substantial robustness. Our approach differs fundamentally, in both methodology and experimental implementation, from existing approaches [8,11], providing a hardware-compatible and efficient route to fast and high-fidelity control of CV systems and bosonic states. Moreover, our framework can be naturally extended to two-qubit logical gates

encoded on bosonic codes by designing two-mode noncommutative Floquet engineering. Our approach can also be applied to applications such as quantum communication [65,66], quantum reservoir computing [67], and quantum t-designs [56,57].

Acknowledgments—T. H. and L. D. acknowledge insightful discussions with R. W. This work was supported by the National Natural Science Foundation of China (Grant No. 12475025). T. H. acknowledges financial support by Knut and Alice Wallenberg through the Wallenberg Center for Quantum Technology (WACQT). L. D. acknowledges financial support by the Knut och Alice Wallenberg stiftelse through Grant No. 2022.0090.

Data availability—The computation code for producing the results in this work is available upon reasonable request.

[1] A. M. Steane, Error correcting codes in quantum theory, Phys. Rev. Lett. **77**, 793 (1996).
[2] G. Q. AI, Suppressing quantum errors by scaling a surface code logical qubit, Nature (London) **614**, 676 (2023).
[3] V. Sivak, A. Eickbusch, B. Royer, S. Singh, I. Tsioutsios, S. Ganjam, A. Miano, B. Brock, A. Ding, L. Frunzio *et al.*, Real-time quantum error correction beyond break-even, Nature (London) **616**, 50 (2023).
[4] J. Lee, N. Kang, S.-H. Lee, H. Jeong, L. Jiang, and S.-W. Lee, Fault-tolerant quantum computation by hybrid qubits with bosonic cat code and single photons, PRX Quantum **5**, 030322 (2024).
[5] S. L. Braunstein and P. van Loock, Quantum information with continuous variables, Rev. Mod. Phys. **77**, 513 (2005).
[6] C. Weedbrook, S. Pirandola, R. García-Patrón, N. J. Cerf, T. C. Ralph, J. H. Shapiro, and S. Lloyd, Gaussian quantum information, Rev. Mod. Phys. **84**, 621 (2012).
[7] S. Lloyd and S. L. Braunstein, Quantum computation over continuous variables, Phys. Rev. Lett. **82**, 1784 (1999).
[8] T. Hillmann, F. Quijandría, G. Johansson, A. Ferraro, S. Gasparinetti, and G. Ferrini, Universal gate set for continuous-variable quantum computation with microwave circuits, Phys. Rev. Lett. **125**, 160501 (2020).
[9] A. M. Eriksson, T. Sépulcre, M. Kervinen, T. Hillmann, M. Kudra, S. Dupouy, Y. Lu, M. Khanahmadi, J. Yang, C. Castillo-Moreno, P. Delsing, and S. Gasparinetti, Universal control of a bosonic mode via drive-activated native cubic interactions, Nat. Commun. **15**, 2512 (2024).
[10] R. W. Heeres, B. Vlastakis, E. Holland, S. Krastanov, V. V. Albert, L. Frunzio, L. Jiang, and R. J. Schoelkopf, Cavity state manipulation using photon-number selective phase gates, Phys. Rev. Lett. **115**, 137002 (2015).
[11] S. Krastanov, V. V. Albert, C. Shen, C.-L. Zou, R. W. Heeres, B. Vlastakis, R. J. Schoelkopf, and L. Jiang, Universal control of an oscillator with dispersive coupling to a qubit, Phys. Rev. A **92**, 040303(R) (2015).
[12] R. W. Heeres, P. Reinhold, N. Ofek, L. Frunzio, L. Jiang, M. H. Devoret, and R. J. Schoelkopf (Google Quantum AI), Implementing a universal gate set on a logical qubit encoded in an oscillator, Nat. Commun. **8**, 94 (2017).
[13] S. Sefi and P. van Loock, How to decompose arbitrary continuous-variable quantum operations, Phys. Rev. Lett. **107**, 170501 (2011).
[14] N. Budinger, A. Furusawa, and P. van Loock, All-optical quantum computing using cubic phase gates, Phys. Rev. Res. **6**, 023332 (2024).
[15] B. C. Travaglione and G. J. Milburn, Preparing encoded states in an oscillator, Phys. Rev. A **66**, 052322 (2002).
[16] J. Niset, J. Fiurášek, and N. J. Cerf, No-go theorem for Gaussian quantum error correction, Phys. Rev. Lett. **102**, 120501 (2009).
[17] M. V. Larsen *et al.*, Integrated photonic source of Gottesman–Kitaev–Preskill qubits, Nature (London) **642**, 587 (2025).
[18] S. Konno, W. Asavanant, F. Hanamura, H. Nagayoshi, K. Fukui, A. Sakaguchi, R. Ide, F. China, M. Yabuno, S. Miki, H. Terai, K. Takase, M. Endo, P. Marek, R. Filip, P. van Loock, and A. Furusawa, Logical states for fault-tolerant quantum computation with propagating light, Science **383**, 289 (2024).
[19] E. Knill and R. Laflamme, Theory of quantum error-correcting codes, Phys. Rev. A **55**, 900 (1997).
[20] A. Joshi, K. Noh, and Y. Y. Gao, Quantum information processing with bosonic qubits in circuit QED, Quantum Sci. Technol. **6**, 033001 (2021).
[21] W. Cai, Y. Ma, W. Wang, C.-L. Zou, and L. Sun, Bosonic quantum error correction codes in superconducting quantum circuits, Fundam. Res. **1**, 50 (2021).
[22] W.-L. Ma, S. Puri, R. J. Schoelkopf, M. H. Devoret, S. Girvin, and L. Jiang, Quantum control of bosonic modes with superconducting circuits, Sci. Bull. **66**, 1789 (2021).
[23] I. Rojkov, M. Simoni, E. Zapusek, F. Reiter, and J. Home, Stabilization of cat-state manifolds using nonlinear reservoir engineering, Phys. Rev. X **16**, 011056 (2026).
[24] L. Guo, T. Huang, and L. Du, Engineering bosonic codes with quantum lattice gates, Commun. Phys. **8**, 414 (2025).
[25] X. C. Kolesnikow, R. W. Bomantara, A. C. Doherty, and A. L. Grimsmo, Gottesman-Kitaev-Preskill state preparation using periodic driving, Phys. Rev. Lett. **132**, 130605 (2024).
[26] J. Emerson, Y. S. Weinstein, M. Saraceno, S. Lloyd, and D. G. Cory, Pseudo-random unitary operators for quantum information processing, Science **302**, 2098 (2003).
[27] M. H. Michael, M. Silveri, R. T. Brierley, V. V. Albert, J. Salmilehto, L. Jiang, and S. M. Girvin, New class of quantum error-correcting codes for a bosonic mode, Phys. Rev. X **6**, 031006 (2016).
[28] P. T. Cochrane, G. J. Milburn, and W. J. Munro, Macroscopically distinct quantum-superposition states as a bosonic code for amplitude damping, Phys. Rev. A **59**, 2631 (1999).
[29] D. Gottesman, A. Kitaev, and J. Preskill, Encoding a qubit in an oscillator, Phys. Rev. A **64**, 012310 (2001).
[30] L. Guo and V. Peano, Engineering arbitrary hamiltonians in phase space, Phys. Rev. Lett. **132**, 023602 (2024).

[31] J. H. Shirley, Solution of the Schrödinger equation with a Hamiltonian periodic in time, Phys. Rev. **138**, B979 (1965).

[32] A. Eckardt and E. Anisimovas, High-frequency approximation for periodically driven quantum systems from a Floquet-space perspective, New J. Phys. **17**, 093039 (2015).

[33] P. Liang, M. Marthaler, and L. Guo, Floquet many-body engineering: topology and many-body physics in phase space lattices, New J. Phys. **20**, 023043 (2018).

[34] See Supplemental Material at http://link.aps.org/supplemental/10.1103/tnb8-3m8m for analytical derivations and additional numerical simulations, which include Refs. [11,12,19,20,24,25,27,29–32,35–46].

[35] J. Urías, Householder factorizations of unitary matrices, J. Math. Phys. (N.Y.) **51**, 072204 (2010).

[36] L. Hu, Y. Ma, W. Cai, X. Mu, Y. Xu, W. Wang, Y. Wu, H. Wang, Y. Song, C.-L. Zou *et al.*, Quantum error correction and universal gate set operation on a binomial bosonic logical qubit, Nat. Phys. **15**, 503 (2019).

[37] E. Knill, R. Laflamme, and L. Viola, Theory of quantum error correction for general noise, Phys. Rev. Lett. **84**, 2525 (2000).

[38] A. Edelman, T. A. Arias, and S. T. Smith, The geometry of algorithms with orthogonality constraints, SIAM J. Matrix Anal. Appl. **20**, 303 (1998).

[39] P.-A. Absil, R. Mahony, and R. Sepulchre, *Optimization Algorithms on Matrix Manifolds* (Princeton University Press, Princeton, NJ, 2008).

[40] K. Zyczkowski and H.-J. Sommers, Induced measures in the space of mixed quantum states, J. Phys. A **34**, 7111 (2001).

[41] M. Mirrahimi, Z. Leghtas, V. V. Albert, S. Touzard, R. J. Schoelkopf, L. Jiang, and M. H. Devoret, Dynamically protected cat-qubits: a new paradigm for universal quantum computation, New J. Phys. **16**, 045014 (2014).

[42] L.-A. Sellem, A. Sarlette, Z. Leghtas, M. Mirrahimi, P. Rouchon, and P. Campagne-Ibarcq, Dissipative protection of a GKP qubit in a high-impedance superconducting circuit driven by a microwave frequency comb, Phys. Rev. X **15**, 011011 (2025).

[43] B. De Neeve, T.-L. Nguyen, T. Behrle, and J. P. Home, Error correction of a logical grid state qubit by dissipative pumping, Nat. Phys. **18**, 296 (2022).

[44] P. Virtanen *et al.* (SciPy 1.0 Contributors), SCIPY1.0: Fundamental algorithms for scientific computing in PYTHON, Nat. Methods **17**, 261 (2020).

[45] M. M. Müller, R. S. Said, F. Jelezko, T. Calarco, and S. Montangero, One decade of quantum optimal control in the chopped random basis, Rep. Prog. Phys. **85**, 076001 (2022).

[46] K. Yi, Y.-J. Hai, K. Luo, J. Chu, L. Zhang, Y. Zhou, Y. Song, S. Liu, T. Yan, X.-H. Deng, Y. Chen, and D. Yu, Robust quantum gates against correlated noise in integrated quantum chips, Phys. Rev. Lett. **132**, 250604 (2024).

[47] H. Moritz, T. Stöferle, M. Köhl, and T. Esslinger, Exciting collective oscillations in a trapped 1D gas, Phys. Rev. Lett. **91**, 250402 (2003).

[48] M. Hofheinz, F. Portier, Q. Baudouin, P. Joyez, D. Vion, P. Bertet, P. Roche, and D. Esteve, Bright side of the coulomb blockade, Phys. Rev. Lett. **106**, 217005 (2011).

[49] Y. Xu and L. Guo, Perturbative framework for engineering arbitrary Floquet Hamiltonian, Rep. Prog. Phys. **88**, 037602 (2025).

[50] M. Suzuki, Generalized Trotter's formula and systematic approximants of exponential operators and inner derivations with applications to many-body problems, Commun. Math. Phys. **51**, 183 (1976).

[51] H. Zhao, M. Bukov, M. Heyl, and R. Moessner, Adaptive trotterization for time-dependent Hamiltonian quantum dynamics using piecewise conservation laws, Phys. Rev. Lett. **133**, 010603 (2024).

[52] Z.-J. Zhang, J. Sun, X. Yuan, and M.-H. Yung, Low-depth Hamiltonian simulation by an adaptive product formula, Phys. Rev. Lett. **130**, 040601 (2023).

[53] P. A. Ivanov, E. S. Kyoseva, and N. V. Vitanov, Engineering of arbitrary U(N) transformations by quantum Householder reflections, Phys. Rev. A **74**, 022323 (2006).

[54] K. Życzkowski and H.-J. Sommers, Average fidelity between random quantum states, Phys. Rev. A **71**, 032313 (2005).

[55] T. Schuster, J. Haferkamp, and H.-Y. Huang, Random unitaries in extremely low depth, Science **389**, 92 (2025).

[56] J. T. Iosue, K. Sharma, M. J. Gullans, and V. V. Albert, Continuous-variable quantum state designs: Theory and applications, Phys. Rev. X **14**, 011013 (2024).

[57] J. Conrad, J. T. Iosue, A. G. Burchards, and V. V. Albert, Continuous-variable designs and design-based shadow tomography from random lattices, Phys. Rev. Lett. **135**, 060802 (2025).

[58] A. M. Childs, Y. Su, M. C. Tran, N. Wiebe, and S. Zhu, Theory of Trotter error with commutator scaling, Phys. Rev. X **11**, 011020 (2021).

[59] C. M. Dawson and M. A. Nielsen, The Solovay–Kitaev algorithm, arXiv:quant-ph/0505030.

[60] M. A. Nielsen, A simple formula for the average gate fidelity of a quantum dynamical operation, Phys. Lett. A **303**, 249 (2002).

[61] L. H. Pedersen, N. M. Møller, and K. Mølmer, Fidelity of quantum operations, Phys. Lett. A **367**, 47 (2007).

[62] Z. Li, P. Liu, P. Zhao, Z. Mi, H. Xu, X. Liang, T. Su, W. Sun, G. Xue, J.-N. Zhang *et al.*, Error per single-qubit gate below 10^{-4} in a superconducting qubit, npj Quantum Inf. **9**, 111 (2023).

[63] E. Hyyppä, A. Vepsäläinen, M. Papič, C. F. Chan, S. Inel, A. Landra, W. Liu, J. Luus, F. Marxer, C. Ockeloen-Korppi, S. Orbell, B. Tarasinski, and J. Heinsoo, Reducing leakage of single-qubit gates for superconducting quantum processors using analytical control pulse envelopes, PRX Quantum **5**, 030353 (2024).

[64] M. Kudra, M. Kervinen, I. Strandberg, S. Ahmed, M. Scigliuzzo, A. Osman, D. P. Lozano, M. O. Tholén, R. Borgani, D. B. Haviland, G. Ferrini, J. Bylander, A. F. Kockum, F. Quijandría, P. Delsing, and S. Gasparinetti, Robust preparation of Wigner-negative states with optimized SNAP-displacement sequences, PRX Quantum **3**, 030301 (2022).

[65] S. Pirandola, U. L. Andersen, L. Banchi, M. Berta, D. Bunandar, R. Colbeck, D. Englund, T. Gehring, C. Lupo, C. Ottaviani *et al.*, Advances in quantum cryptography, Adv. Opt. Photonics **12**, 1012 (2020).

[66] L. Wang, G. Chai, Z. Cao, and X. Chen, Highly reliable quantum secure direct communication based on concatenated GKP-QLDPC codes, Sci. China Inf. Sci. **69**, 179403 (2026).

[67] J. Dudas, B. Carles, E. Plouet, F. A. Mizrahi, J. Grollier, and D. Marković, Quantum reservoir computing implementation on coherently coupled quantum oscillators, npj Quantum Inf. **9**, 64 (2023).

[68] Z. Wu, L. Guo, H. Shi, and W.-W. Zhang, Autonomous Floquet engineering of bosonic codes via reinforcement learning, arXiv:2510.22227.

End Matter

Beyond adiabaticity—Previous works prepared bosonic code states using Hamiltonian Floquet engineering combined with adiabatic ramping (AR) [24,25]. In those protocols, periodic driving is used to mimic an effective Hamiltonian whose eigenstates encode the logical code states, and a slowly varying ramp then prepares the target state (i.e., an arbitrary superposition of the logical code states) from a suitably chosen initial state (with nonzero overlap with the target state) via adiabatic evolution. However, it has been shown that AR protocols typically require evolution over *thousands* of driving periods to achieve high fidelity [24,25]. Even with machine-learning-assisted optimization [68], the protocol remains slow and is therefore vulnerable to decoherence and control noise on current hardware.

Our single-period Floquet (SF) approach goes beyond this paradigm by abandoning AR altogether. Instead, it directly synthesizes a target unitary that prepares the desired state from an arbitrary initial state within a single Floquet period. As a result, the SF method dramatically reduces the control time and exhibits substantially improved robustness under realistic noise conditions [34]. When further combined with optimal pulse engineering, it achieves even higher accuracy without sacrificing its short-duration advantage.

In Table I, we benchmark the performance of the SF and AR methods, as well as their optimized variants, in terms of timescale, state-preparation fidelity, and robustness under identical noisy environments. Here, robustness is defined as the maximum tolerable noise strength for achieving high-fidelity (> 0.99) code-state preparation under the same noise model (see the Supplemental Material [34] for detailed numerical setup and the full robustness analysis). Overall, our SF method significantly outperforms the AR protocol, yielding improvements of up to three orders of magnitude across all considered metrics.

Controllability benchmark—Universal control of a CV logical qubit can be realized by combining displacement operations with SNAP gates in a resonator-qubit architecture [11,12]. Since these operations act primarily on the resonator and the ancillary qubit, respectively, they are typically applied sequentially [11]. This gate set provides a standard building block for arbitrary CV control in truncated Hilbert spaces, with full $\mathbb{U}(d)$ controllability demonstrated experimentally in circuit QED [12]. We therefore benchmark the QLG circuit and the following L-layer SNAP circuit:

$$\hat{\mathcal{C}}_{SNAP} = \prod_{\ell=1}^{L}\left[\hat{\mathcal{D}}(\alpha_\ell)\prod_{j=1}^{d}\hat{S}(\vartheta_{j,\ell})\right], \tag{B1}$$

$$\hat{\mathcal{C}}_{\mathrm{qlg}} = \prod_{n=1}^{N_t}\hat{\mathbf{G}}[\vec{\beta}(t_n)]. \tag{B2}$$

Here, $\hat{\mathcal{D}}(\alpha)$ denotes the displacement operator and $\hat{S}(\vartheta)$ is the SNAP gate. Since $\alpha \in \mathbb{C}$ is complex and bounded by $|\alpha| \le \alpha_{\max}$, each displacement contributes two real parameters (its real and imaginary parts). Therefore, the SNAP circuit contains $L \times (d+2)$ trainable real parameters, whereas the QLG circuit contains N_t trainable parameters.

To quantify controllability under finite circuit complexity, we benchmark the preparation of Haar-random target states in a truncated Hilbert space of dimension d. Here $\mathcal{R}$ denotes the number of trainable parameters, and we define the computational resources for optimization as the minimal number of parameters required to reach a target infidelity threshold ε,

$$\mathcal{R}_{\min}(d;\varepsilon) \coloneqq \min\{\mathcal{R} | 1 - \mathcal{F}^{\star}_{\mathcal{C}}(\mathcal{R},d) \le \varepsilon\}, \tag{B3}$$

TABLE I. Benchmark comparison of our SF method with AR approach for bosonic code-state preparation. We compare the required preparation time (in units of the Floquet period), the achieved infidelity, and the robustness under identical noise conditions. Here, the robustness is defined as the maximum tolerable noise strength for maintaining high-fidelity (> 0.99) code-state preparation. The machine-learning-assisted AR (AR + ML) method and SF method with optimal pulse engineering (SF + OPE) are also included in the comparison.

Methods	Time	Infidelity	Robustness
AR [24,25]	$\sim 10^3$	10^{-2}	10^{-3}
AR + ML [68]	$\sim 10^2$	10^{-2}	…
SF (this Letter)	$\mathcal{O}(1)$	10^{-2}	10^{-2}
SF + OPE (this Letter)	$\mathcal{O}(1)$	10^{-5}	10^{-1}

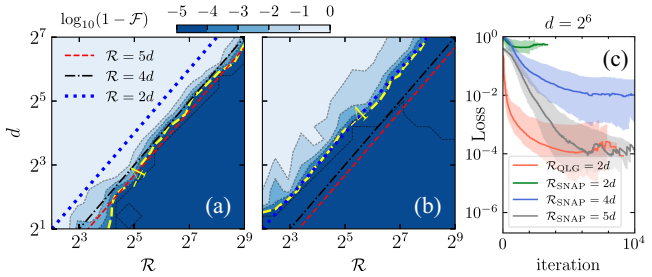

FIG. 4. Controllability benchmark. Average infidelity for preparing 10^2 Haar-random target states as a function of the Hilbert-space dimension d and the number of trainable parameters $\mathcal{R}$. Results for the SNAP- and QLG-based circuits are shown in panels (a) and (b), respectively. The thick yellow dashed curve marks the contour $\log_{10}(1-\mathcal{F}) \simeq -4$, while the other dotted and dashed guide lines indicate linear scalings $\mathcal{R} = 2d, 4d, 5d$. (c) Training dynamics for $d = 2^6$, showing the loss versus iteration under the same optimization setup for several parameter budgets. Parameters: $\delta = 2$ and $\alpha_{\max} = \sqrt{d}$.

where $\mathcal{F}^{\star}_{\mathcal{C}}(\mathcal{R}, d)$ is the optimized fidelity achievable by a circuit *Ansatz* $\mathcal{C}$ with $\mathcal{R}$ trainable parameters. In our numerics, the $\mathcal{R}$ trainable parameters are assigned by including all parameters from the first several complete SNAP layers, while any remaining parameters, if needed, are randomly sampled from the subsequent layer. Further details of the optimization procedure are provided in SM [34].

Figure 4 shows the average optimized infidelity as a function of d and $\mathcal{R}$ for the SNAP- and QLG-based circuits. The yellow dashed contour marks the threshold $\varepsilon \simeq 10^{-4}$ and therefore directly reveals the scaling of the minimal resource cost.

As shown in Figs. 4(a) and 4(b), the fixed-infidelity contour (yellow dashed) exhibits qualitatively different scaling behaviors for the two circuit *Ansätze*,

$$\mathcal{R}^{\mathrm{qlg}}_{\min}(d; 10^{-4}) \sim 2d, \qquad \mathcal{R}^{SNAP}_{\min}(d; 10^{-4}) \sim 5d. \tag{B4}$$

Thus, to achieve the same target accuracy, the QLG *Ansatz* requires substantially fewer trainable parameters as the Hilbert-space dimension increases. We attribute this favorable scaling to the analytical construction underlying the QLG method, which provides an accurate closed-form initialization and thereby reduces the subsequent optimization burden. This interpretation is supported by the close agreement between the fidelities of the bare and optimized QLG protocols, as shown in Figs. 2(a) and 4(b). This is further consistent with the training dynamics in Fig. 4(c), where the QLG protocol converges more efficiently under the same optimization setup [34].